Journal Name

ARTICLE TYPE

Cite this: DOI: 10.1039/xxxxxxxxxx

Hindered rotor tunneling splittings: an application of the two-dimensional non-separable method to benzyl alcohol and two of its fluorine derivatives†

Tiago Vinicius Alves[a], Luis Simón-Carballido[b], Fernando Rei Ornellas[a] and Antonio Fernández-Ramos*[b]

Received Date
Accepted Date

DOI: 10.1039/xxxxxxxxxx

www.rsc.org/journalname

In this work we present a novel application of the two-dimensional non-separable (2D-NS) method to the calculation of torsional tunneling splittings in systems with two hindered internal rotors. This method could be considered an extension of one-dimensional methods for the case of two compound tops. The 2D-NS method includes coupling between torsions in the kinetic and potential energy. Specifically, it has been applied to benzyl alcohol (BA) and two of its fluorine derivatives: 3-fluorobenzyl alcohol (3FBA) and 4-fluorobenzyl alcohol (4FBA). These molecules present two torsions, i.e., about the -CH_2OH (ϕ_1) and -OH (ϕ_2) groups. The electronic structure calculations to build the two-dimensional torsional potential energy surface were performed at the DF-LMP2-F12//DF-LMP2/cc-pVQZ level of theory. For BA and 4FBA the calculated ground-state vibrational level splittings are 429 and 453 MHz, respectively, in good agreement with the experimental values of 337.10 and 492.82 MHz, respectively. In these two cases there are four equivalent wells and the tunneling splitting is the result of transitions between the two closer minima along ϕ_1. The analysis of the wavefunctions, as well as the previous experimental work on the system, supports this conclusion. For 3FBA the observed ground-state splitting is 0.82 MHz, whereas in this case the calculated value amounts only to 0.02 MHz. The 2D-NS method, through the analysis of the wavefunctions, shows that this tiny tunneling splitting occurs between the two most stable minima of potential energy surface. Additionally, we predict that the first vibrationally excited tunneling splitting will also be small and exclusively due to the interconversion between the second lowest minima.

1 Introduction

Tunneling splittings are associated to a quantum mechanical effect which makes energy levels to split into doublets, triplets, quadruplets, etc., due to the overlapping in the classically forbidden region of wave functions of identical wells. At low temperatures, tunneling is the only mechanism through which a molecule can reach another potential well, since it has not enough energy to overcome the potential barrier. Tunneling is very sensitive to the mass of the particle that penetrates through the potential barrier and to the width of such a barrier, in a way that this quantum effect becomes more important for light particles (as for instance protons and hydrogen atoms) passing through narrow barriers. It should be noticed that tunneling splittings are physical observables and can be measured using different experimental techniques. In fact, zero-point and selected mode-specific tunneling splittings due to proton transfer reactions have been observed in several molecules with symmetric double-well potentials. Malonaldehyde[1] is a classic example with a zero-point splitting of 21.6 cm^{-1}. From the theoretical point of view, this effect was firstly described by Hund[2], and nowadays, there is a wide variety of multidimensional methods that can deal accurately with the observed tunneling splittings due to proton transfer[3–9] or to the flip of clusters.[10]

Less attention has been paid to the study of tunneling splittings that may arise from internal rotations, although there are notable exceptions.[11] Tunneling occurs when a flexible molecule with one or more hindered rotations (i.e., torsions about single bonds with a given energetic barrier) is able to reach a different well of the torsional potential by penetration through the torsional barrier.

† Electronic Supplementary Information (ESI) available: See DOI: 10.1039/b000000x/

[a] Departamento de Química Fundamental, Instituto de Química, Universidade de São Paulo, Av. Prof. Lineu Prestes 748, São Paulo, SP, 05508-000, Brazil

[b] Department of Physical Chemistry and Center for Research in Biological Chemistry and Molecular Materials (CIQUS), University of Santiago de Compostela, 15782 Santiago de Compostela, Spain

* Electronic mail: qf.ramos@usc.es

For molecules with one torsional mode and two wells with the same energy, the energy levels below the barrier may split into a doublet, being one of the components symmetric (+) and the other antisymmetric (−) with respect to that torsional mode (the reaction coordinate). If there are more than two wells, we may encounter more complicated patterns than just doublets.

The vibrational ground state level ($\upsilon_1 = 0$, $\upsilon_2 = 0$) of molecules with two rotating groups and torsional coordinates ϕ_1 and ϕ_2 may also split, but the number of spectral lines will depend on the characteristics of the system. Caminati and coworkers[12] obtained the rotational spectra of benzyl alcohol (BA) using pulsed-jet Fourier transform microwave and free jet absorption millimeter spectroscopy. These authors observed b-type transitions separated by 986 MHz, which correspond to a splitting of vibrational ground-state of 492.8 MHz. The same research group measured the vibrational-ground state tunneling splittings of 3-fluorobenzyl alcohol[13] (3FBA) and of 3, 4-difluorobenzyl alcohol[14] (3,4DFBA), this time due to c-type transitions. Their results indicated that the asymmetry generated by the replacement of a hydrogen atom by a fluorine atom in the *meta* position of the phenyl ring practically annihilates the tunneling splitting. These splittings are much smaller than that of benzyl alcohol, i.e., 0.82 and 0.13 MHz for 3FBA and 3,4DFBA, respectively. Another fluorine derivative of the benzyl alcohol was studied by Bird *et al.*[15] who obtained the rotationally resolved electronic spectra of 4-fluorobenzyl alcohol (4FBA) and a ground state tunneling splitting of 337.10 MHz.

Our theoretical study is focused on BA, 3FBA and 4FBA, which are systems involving compound rotation (one rotating group attached to another rotating group). Kilpatrick and Pitzer[16] found that accurate thermodynamic functions for flexible molecules of this type can be obtained from partition functions in which the torsional modes are treated as coupled anharmonic hindered rotors and the remaining vibrational modes as harmonic oscillators. We have extended the methodology developed by Kilpatrick and Pitzer to low temperatures for system with two rotors by directly solving the two-dimensional Schrödinger equation. We call this approximation two-dimensional non-separable (2D-NS)[17] and it has been used recently for the calculation of quantum hindered rotor partition functions.[17,18] It incorporates full coupling between torsions in both kinetic and potential energy. In this work we use this methodology to calculate tunneling splittings arising from hindered rotations.

Previous theoretical calculations on some of these systems carried out by Caminati and coworkers[12,13] were limited to one-dimensional models, which can be considered as a particular case of the two-dimensional problem. Those authors have chosen as tunneling path the one passing through the transition states connecting the minima, but either they had to modify the calculated parameters or to scale the potential in order to match the observed tunneling splittings. This indicates that one-dimensional methods are unreliable, and without any adjustment, the results may differ from the experimental values by more than an order of magnitude. The theoretical calculation of tunneling splittings using a prescribed one-dimensional coordinate involves the following steps: (i) evaluation of the one-dimensional potential about the path; (ii) fitting of the potential, V(ϕ), to Fourier series; and (iii) resolution of the Schrödinger equation of the type:

$$-\frac{\hbar}{2I}\frac{d^2}{d\phi^2}\Phi(\phi)+V(\phi)\Phi(\phi)=E\Phi(\phi) \qquad (1)$$

where $\hbar = h/2\pi$, h is the Planck constant; I is the reduced moment of inertia due to the rotating group and $\Phi(\phi)$ is the wavefunction. For the systems mentioned above ϕ describes a full revolution about the rotation attached to the molecular frame (hereafter ϕ_1), but depending on the path, the other torsion (hereafter ϕ_2) may take different values.

Torsions ϕ_1 and ϕ_2 define a two-dimensional potential energy surface, so to solve the Schrödinger equation in two dimensions using the 2D-NS method avoids a difficult search for the optimum path for tunneling. In this method the potential is expressed as a Fourier series expansion and the resulting Hamiltonian is introduced in the Schrödinger equation, which is solved by the variational method. The objective of this work is to show that 2D-NS is a benchmark method for the calculation of tunneling splittings arising from hindered rotations in molecules with two tops. This methodology does not involve any empirical adjustment of the potential energy surface beyond the choice of the level of the electronic structure calculations, so it could be used as a tool to predict tunneling splittings. Additionally, through the analysis of the wavefunctions, the 2D-NS method can identify which are the wells and the torsional motions that lead to the observed tunneling splitting. This is important because BA and 4FBA present four wells with the same energy and it is not completely established which are the internal rotations that generate the tunneling splittings.

Section 2 briefly describes the 2D-NS method (see Ref. 17 for details). Computational details are given in Section 3. Section 4 discusses the energetic and structural parameters of the torsional potential energy surface of the three systems, as well as, the results obtained by the 2D-NS method. Additionally, splittings are also calculated with Eq. 1 for comparison. Section 5 summarizes the conclusions.

2 Methodology

The Hamiltonian of the 2D-NS method for a molecule with two hindered rotors ϕ_1 and ϕ_2 can be written as:[17]

$$H_{\mathrm{tor}}\left(\frac{\partial}{\partial\phi_1},\frac{\partial}{\partial\phi_2};\phi_1,\phi_2\right)=T_{\mathrm{tor}}\left(\frac{\partial}{\partial\phi_1},\frac{\partial}{\partial\phi_2}\right)+V_{\mathrm{tor}}(\phi_1,\phi_2) \qquad (2)$$

where the kinetic operator, T_{tor}, is given by:

$$T_{\mathrm{tor}}\left(\frac{\partial}{\partial\phi_1},\frac{\partial}{\partial\phi_2}\right)=-\frac{\hbar}{2}\sum_{\tau=1}^{2}\sum_{\varsigma=1}^{2}d_{\tau\varsigma}\frac{\partial^2}{\partial\phi_\tau\partial\phi_\varsigma}+\frac{\partial d_{\tau\varsigma}}{\partial\phi_\tau}\frac{\partial}{\partial\phi_\varsigma} \qquad (3)$$

and the elements $d_{\tau\varsigma}$, $\tau = 1,2$; $\varsigma = 1,2$ are those the inverse matrix:

$$[\mathbf{D}(\phi_1,\phi_2)]^{-1} = \frac{1}{|\mathbf{D}(\phi_1\phi_2)|}\begin{pmatrix} I_2(\phi_1,\phi_2) & \Lambda_{1,2}(\phi_1,\phi_2) \\ \Lambda_{1,2}(\phi_1,\phi_2) & I_1(\phi_1,\phi_2) \end{pmatrix} = \begin{pmatrix} d_{11} & d_{12} \\ d_{12} & d_{22} \end{pmatrix} \quad (4)$$

where $|\mathbf{D}(\phi_1\phi_2)|$ is the determinant of the $\mathbf{D}$ matrix; $I_1(\phi_1,\phi_2)$ and $I_2(\phi_1,\phi_2)$ are the reduced moments of inertia and $\Lambda_{1,2}(\phi_1,\phi_2)$ is the coupling between torsions. These quantities were calculated by the method developed by Kilpatrick and Pitzer.[16]

The electronic structure data are fitted to a Fourier series of the type:

$$\begin{aligned} V_{\mathrm{tor}}(\phi_1,\phi_2) =& V_1(\phi_1)+V_2(\phi_1)+ \\ & \sum_{L_1=1}^{L_{1,max}}\sum_{L_2=1}^{L_{2,max}} c_{L_1L_2}\cos(L_1\phi_1)\cos(L_2\phi_2)+ \\ & \sum_{P_1=1}^{P_{1,max}}\sum_{P_2=1}^{P_{2,max}} d_{P_1P_2}\sin(P_1\phi_1)\sin(P_2\phi_2)+ \\ & \sum_{L'_1=1}^{L'_{1,max}}\sum_{L'_2=1}^{L'_{2,max}} c'_{L'_1L'_2}\cos(L'_1\phi_1)\sin(L'_2\phi_2)+ \\ & \sum_{P'_1=1}^{P'_{1,max}}\sum_{P'_2=1}^{P'_{2,max}} d'_{P'_1P'_2}\sin(P'_1\phi_1)\cos(P'_2\phi_2) \end{aligned} \quad (5)$$

where $c_{L_1L_2}, L_1 = 1,...,L_{1,max}, L_2 = 1,...,L_{2,max}, d_{P_1P_2}, P_1 = 1,...,P_{1,max}, P_2 = 1,...,P_{2,max}$, $c'_{L'_1L'_2}, L'_1 = 1,...,L'_{1,max}, L'_2 = 1,...,L'_{2,max}, d'_{P'_1P'_2}, P'_1 = 1,...,P'_{1,max}, P'_2 = 1,...,P'_{2,max}$ are fitting parameters, and $L_{1,max}$, $L'_{1,max}$, $L_{2,max}$, $L'_{2,max}$, $P_{1,max}$, $P_{2,max}$, $P'_{1,max}$, and $P'_{2,max}$ indicate the largest number of each series. The one-dimensional potentials are:

$$V_1(\phi_1) = a_0 + \sum_{M=1}^{M_{max}} a_M\cos(M\phi_1) + \sum_{M'=1}^{M'_{max}} a'_{M'}\sin(M'\phi_1) \quad (6)$$

and

$$V_2(\phi_2) = b_0 + \sum_{N=1}^{N_{max}} b_N\cos(N\phi_2) + \sum_{N'=1}^{N'_{max}} b'_{N'}\sin(N'\phi_2) \quad (7)$$

where, a_0, b_0, $a_M(M = 1,...,M_{max})$, $a'_{M'}(M' = 1,...,M'_{max})$, $b_N(N = 1,...,N_{max})$, $b'_{N'}(N' = 1,...,N'_{max})$ are fitting parameters, and M_{max}, M'_{max}, N_{max}, and N'_{max} are the largest number of each series. Once the number of terms for each of series of Eq. 5 are known, the same type of series are used to fit each of the elements of the inverse of the $\mathbf{D}(\phi_1\phi_2)$ matrix of Eq. 4. All parameters are given in the Supplementary Information.

The trial wavefunction used to solve the Schrödinger equation

$$H_{\mathrm{tor}}\left(\frac{\partial}{\partial\phi_1},\frac{\partial}{\partial\phi_2};\phi_1,\phi_2\right)\Phi(\phi_1,\phi_2) = E\Phi(\phi_1,\phi_2) \quad (8)$$

using the Hamiltonian of Eq. 2, can be written as the product of two one-dimensional functions, and each of them is a linear combination of wavefunctions which are solution of Schödinger equation for the particle in a ring:

$$\Phi(\phi_1,\phi_2) = \Phi_1(\phi_1)\Phi_2(\phi_2) \quad (9)$$

where,

$$\Phi_1(\phi_1) = \frac{1}{\sqrt{2\pi}}\sum_{k=-k_{\max}}^{k=k_{\max}} c_{1,k}e^{ik\phi_1}, \quad (10)$$

and

$$\Phi_2(\phi_2) = \frac{1}{\sqrt{2\pi}}\sum_{n=-n_{\max}}^{n=n_{\max}} c_{2,n}e^{ik\phi_2}, \quad (11)$$

The lowest eigenvalues and wavefunctions calculated from Eq. 8 are the ones of interest, and the results are discussed in Section 4. Details about the matrix elements of the Hamiltonian are given in Ref. 17.

3 Computational Details

The geometry optimization of all the stationary points was carried out at the density fitted local MP2 (DF-LMP2)[19,20] method with the initial Hartree-Fock orbital optimization calculated using the DF-HF method[21] and the correlation consistent valence quadruple-zeta cc-pVQZ basis set.[22] The corresponding auxiliary basis sets cc-pVQZ/MP2 and cc-pVQZ/JKFIT of Weigend *et al.*[23,24] were employed in the DF-LMP2 and DF-HF calculations, respectively. The two-dimensional torsional potential energy surfaces of BA, 3FBA and 4FBA were generated by full optimization of all the degrees of freedom but the two torsions. The two torsions were scanned using a stepsize of 10°. At each step, single point DF-LMP2-F12[25–27] calculations were performed to compute accurate second-order correlation energies. Hereafter, torsions ϕ_1 and ϕ_2 refer to torsions about the OC-CC and HO-CC single bonds, respectively. The geometries of the minima of BA, 3FBA and 4FBA are given in the Supplementary Information.

The potential energy grid obtained from the electronic structure calculations was fitted to Fourier series using the GNUPlot program.[28] The fit was considered satisfactory when the root mean square of residuals was smaller than 1 cm^{-1}. The one-dimensional and the coupling parameters used in Eq. 5, as well as those parameters used in the fitting of the kinetic energy, are listed in the Supplementary Information. The calculation of the lowest eigenvalues and the corresponding eigenvectors was carried out with the help of the JADAMILU software library.[29] All electronic structure calculations were carried out with the MOLPRO 2010[30] suite of programs.

4 Results and Discussion

Table 1 indicates the values of ϕ_1 and ϕ_2 at the minima calculated at the DF-LMP2-F12//DF-LMP2/cc-pVTZ level for the BA, 4FBA and 3FBA systems. A representation of the minima of 3FBA and 4FBA is given in Figure 1. In the case of 3FBA, the scan about the two asymmetric tops leads to a two-dimensional potential energy

surface with six wells of which only four wells are distinguishable, as shown in Figure 2. The most stable minimum, 3FBA-M1, is located at dihedrals $[\phi_1, \phi_2]$ equal to [43, 58] whereas in the case of 3FBA-M2 they are located at [135,-57]; the former is 47 cm^{-1} more stable than the latter. Each of the two structures has one enantiomer (3FBA-M1* and 3FBA-M2*) as shown in Figure 1. Hereafter, enantiomers are labeled with asterisk. The values of the torsional angles at the equilibrium structures calculated by Tang *et al.* [13] are close to the values obtained in this study. However, there are discrepancies related to the nature of the 3FBA-M3 and 3FBA-M4 stationary points, located at dihedrals [0, 180] and [180, 180], respectively. In the work of Tang *et al.* [13] those stationary points are transition states, but our electronic structure calculations show that they are minima. Actually, the relative energies calculated by them are much closer to the transition state energies obtained in this work than to the energies of the minima (see Table 2). The transition states for the torsions M1→M3 and M2→M4 have energies of 525 and 535 cm^{-1}, which are close to the transition state energies of torsions M1→M1* and M2→M2* described by Tang *et al.* [13] (with energies of 515 and 585 cm^{-1}). This shows that the interconversion from 3FBA-M1 to 3FBA-M1* is a two step-process with an intermediate well located at 3FBA-M3. The same circumstance occurs for the interconversion between 3FBA-M2 and 3FBA-M2*, but in this case the intermediate is 3FBA-M4.

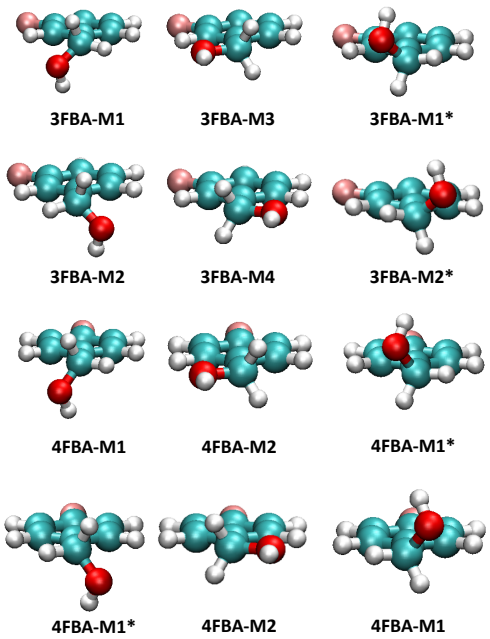

Fig. 1 Ball and stick representation of the equilibrium geometries of 3FBA and 4FBA listed in Table 1. The geometries of BA are very similar to those of 4FBA, so they are not plotted. Light gray, red, brown and cyan represent hydrogen, oxygen, fluorine and carbon atoms, respectively.

The torsional potential energy surface for the 4FBA is also illustrated in the Figure 2. For BA the potential is not plotted because it is very similar to that of 4FBA. The substituted benzene ring in the *para* position changes the nature of the wells, because now the molecule has symmetry with respect to the internal rotation about ϕ_1. Any structure with torsions $[\phi_1, \phi_2]$ is equivalent to another structure with torsions $[\phi_1 + 180, \phi_2]$, so the molecule presents a C_2 axes for internal rotation through the -C-CH_2OH single bond. The torsion about this chemical bond generates two indistinguishable minima 4FBA-M1 and each of them has one enantiomer 4FBA-M1*. This leads to a potential energy surface with four isoenergetic wells. The torsional internal angles at the equilibrium geometry of 4FBA-M1 and 4FBA-M1* are in good agreement with the four wells identified at the M05-2X/6-31+G(d,p) level by Bird *et. al* [15]. There are also two indistinguishable wells at positions [0, 180] and [180, 180], which correspond to the 4FBA-M2 wells and are 351 cm^{-1} above the 4FBA-M1 wells. In the case of BA the calculated barrier height by Utzat *et. al* [12] at the CBS extrapolation limit between BA-M1 and BA-M1* is 319 cm^{-1}, which is in very good agreement with the DF-LMP2-F12//DF-LMP2/cc-pVQZ barrier height. The minima and the transition states for BA and 4FBA have similar energetics, although the lowest rotational barrier in BA is 42 cm^{-1} smaller than the same barrier in 4FBA. This may be the reason why the tunneling splitting in BA is larger than that in 4FBA.

Im *et al.* [31] indicated that the torsional potential energy surface in benzyl alcohols is a combination of two factors: (i) the interaction between the -CH_2OH group and the hydrogen atoms located at the *ortho* position of the ring and (ii) the interaction between the hydroxyl group and the π-electrons of ring. The first interaction is repulsive and more important when the -CH_2OH group is in eclipsed position ($\phi_1 = 0°$) with respect to the ring. On the other hand the attractive interaction between the -OH group and the π-electron cloud of the ring is favored at large values of ϕ_1 with the hydrogen atom of the hydroxyl group pointing toward the ring. On the basis of these two interactions and on spec-

Table 1 Dihedral angles $[\phi_1, \phi_2]$ (in degrees) and relative energies U_i (in cm^{-1}) of the minima of 3FBA and 4FBA obtained at the DF-LMP2-F12//DF-LMP2/cc-pVQZ level. Results in parentheses for 3FBA, 4FBA and BA are taken from Ref. 13, Ref. 15 and Ref. 12, respectively.

System	Well	$[\phi_1,\phi_2]$	U_i
3FBA	M1 (Z)	[43, 58], ([49,56])	0 (0)
	M1* (Z')	[-43, -58], ([-49,-56])	0 (0)
	M2 (E)	[135,-57], ([129,-55])	47 (27)
	M2* (E')	[-135,57], ([-129,55])	47 (27)
	M3	[0,180]	279 (—)
	M4	[180,180]	343 (—)
4FBA	M1	[53, 54], [-127, 54]	0
		([44, 57], [-136, 57])	(0)
	M1*	[-53, -54], [127, -54]	0
		([-44, -57], [136, -57])	(0)
	M2	[0, 180], [180, 180]	351
BA	M1	[53, 53], [-127, 53]	0
		([55, 65], [-125, 65])	(0)
	M1*	[-53, -53], [127, -53]	0
		([-55, -65], [125, -65])	(0)
	M2	[0, 180], [180, 180]	403

Table 2 Same as Table 1, but for the transition states with the lowest energy.

System	TS	$[\phi_1,\phi_2]$	U_i
3FBA	M1→M3	[0, 125]	525
	M3→M1*	[0, -125]	246
	(M1→M1*)	([0, 180])	(515)
	M2→M4	[174, 124]	535
	M4→M2*	[-174, -124]	192
	(M2→M2*)	([180, 180])	(585)
	M1→M2	[90, 0]	452 (509)
	M1*→M2*	[-90, 0]	452 (509)
4FBA	M1→M1*	[90, 0], [-90, 0]	371 (304)
	M1→M1	[136, 80], [-44, 80]	721
	M1*→M1*	[-136, -80], [44, -80]	721
	M1→M2	[6, 122], [-174,122]	603
	M2→M1*	[174, -122], [-6, -122]	603
BA	M1→M1*	[90, 0], [90, 0]	329 (319)
	M1→M1	[137, 75], [-43, 75]	705
	M1*→M1*	[-137, -75], [43, -75]	705
	M1→M2	[7, 123], [-173,122]	635
	M2→M1*	[173, -123], [-7, -123]	635

troscopy studies, Im *et al.*[31] concluded that for these substituted benzyl alcohols, the wells should be located at $\phi_1 = 90°$ (i.e., with the OH perpendicular to the ring). However, our theoretical calculations, and those carried out by Tang *et al.*[13] and by Bird *et. al*[15], indicate that -OH group with respect to the ring is closer to a *gauche*-type position. The hydrogen of the -OH group points toward the ring except for the minima in which $\phi_1 = 0°$, because of the repulsion with the *ortho* hydrogen atoms.

The agreement between calculated and experimental rotational constants is good (see Table 3). The reduced moment of inertia for the internal rotation of the -CH_2OH group is about 20 times larger than that of the -OH group. The moment of inertia in rotational motion meets the same purpose as the mass in the linear motion, and therefore their values have an important effect on the magnitude of the tunneling splittings. Notice that the tunneling effect is affected by the shape of the potential barrier between the wells (width and height) and by the mass (or moment of inertia in rotational motion) of the tunneling particle. In the case of BA and 4FBA, if we assume that the barriers M1→M1 and M1→M1* are isoenergetic, the former transit would have a much lower tunneling splitting because it involves a larger rearrangement of the

Table 3 Rotational constants (in MHz) of all conformers of 3FBA, 4FBA and BA (experimental values in parentheses). Reduced moments of inertia I_1, I_2 in amu Å^2.

System	Conformer	A,B,C	I_1, I_2
3FBA	3FBA-M1	2804, 1210, 870	18.02, 0.830
	3FBA-M1	(2757, 1210, 863)[a]	—
	3FBA-M2	3413, 1067, 842	19.59, 0.824
	3FBA-M3	2679, 1231, 848	16.06, 0.826
	3FBA-M4	3571, 1038, 810	18.13, 0.830
4FBA	4FBA-M1	4648, 932, 808	17.64, 0.825
	4FBA-M1	(4629, 929, 803)[b]	—
	4FBA-M2	4770, 945, 793	16.61, 0.805
BA	BA-M1	4787, 1480, 1192	16.89, 0.823
	BA-M1	(4759, 1475, 1193)[c]	—
	BA-M2	4959, 1504, 1163	15.38, 0.800

[a] Ref. 13
[b] Ref. 15
[c] Ref. 12

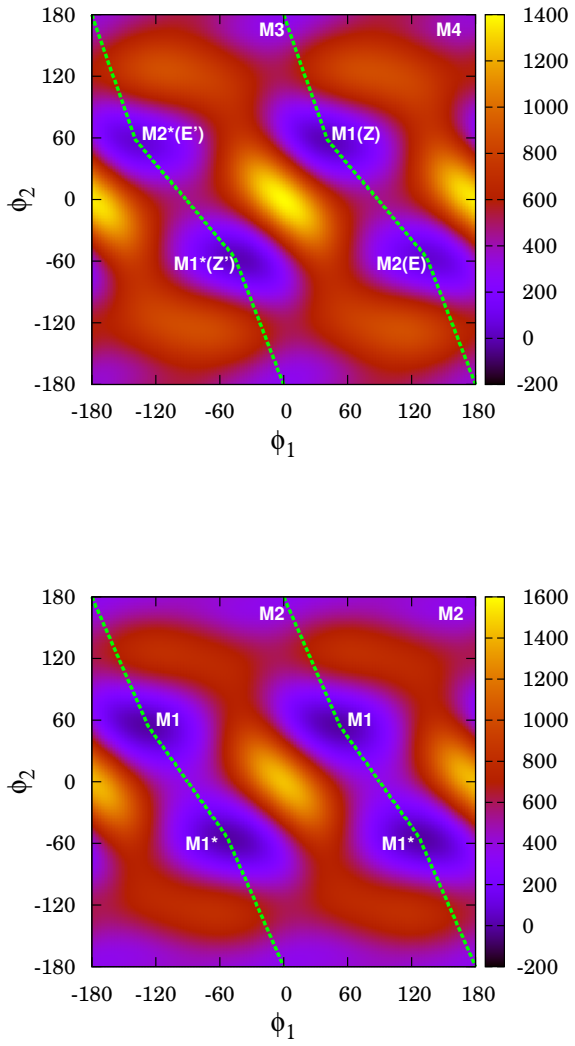

Fig. 2 Contour plots of the potential energy surface resulting from the rotation about the torsional angles ϕ_1 and ϕ_2 for 3FBA (top) and 4FBA (bottom). The location of the minima is indicated. The green lines show the linear reaction path.

ϕ_1 dihedral (i.e. 180° for the former and 74° for the latter).

The tunneling splitting can also be calculated from the path that minimizes the Euclidean action. This tunneling trajectory, which is the best compromise between paths of varying length and height, is called *instanton*. One of us have used two approximate methods based in this methodology to calculate tunneling splittings in several proton transfer reactions.[3,8,32–35] In this case, we directly solve the two-dimensional Schrödinger equation of Eq. 8 to obtain the eigenvalues and the tunneling splittings listed in Table 4.

As we have mentioned in the Introduction Section, it is possible to solve the one-dimensional Schrödinger equation of Eq. 1 using a potential which is a function of the two torsions and with all the other degrees of freedom relaxed. In a compound rotation

this path should involve a full rotation about the OC-CC single bond (ϕ_1), but it is not clear how to proceed with the HO-CC torsion (ϕ_2) to obtain the optimum tunneling path. As shown in Figure 2 the minima are located not only at different values of ϕ_1, but also of ϕ_2 because both torsions are strongly coupled. To evaluate the tunneling splittings along a one-dimensional trajectory we have chosen the linear reaction path, which is the shortest path between minima. These potentials are plotted in Figure 3 for the three systems. The tunneling splittings were obtained via Eq. 1 using as reduced moment of inertia the one of ϕ_1 at the global minimum, and as potential a cosine Fourier series that fits the one-dimensional potential. The calculated values for 3FBA, 4FBA and BA are 0.26, 2.75 and 44.8 MHz, respectively, which are substantially smaller than the experimental values. These results show that one-dimensional methods have difficulty providing tunneling splittings of the same order of magnitude as the experimental values if empirical parameters are not used. Even if the linear reaction path is the best choice to calculate the tunneling splitting, the results may not be accurate because of the kinetic energy term, which should somehow include the coupling between torsions. For instance, the above result can be improved if the reduced moment of inertia I_1 is substituted in Eq. 1 by an effective reduced moment of inertia $I_{\rm eff}$ which accounts for the variation of the two torsions ($\Delta\phi_1$ and $\Delta\phi_2$) along the linear reaction path between the minima that lead to the tunneling splitting:

$$I_{\rm eff} = \frac{I_1|\Delta\phi_1| + I_2|\Delta\phi_2|}{\sqrt{\Delta\phi_1^2 + \Delta\phi_2^2}} \qquad (12)$$

With this modification the tunneling splittings for 3FBA, 4FBA and BA are 0.30, 117 and 965 MHz, respectively, which are in much better agreement with experiment. The problem is that Eq. 12 is an empirical expression, which may not work in other cases, as for instance if the chosen tunneling path is far from the linear reaction path. These results indicate that one-dimensional methods for the study of compound rotations have limited accuracy, because it is difficult to estimate the coupling between torsions. However, this term can be easily evaluated within the 2D-NS approach. Therefore, if we can afford the construction of the two-dimensional potential energy surface, it is better to directly solve the two-dimensional Schrödinger equation by the 2D-NS method than search for the best tunneling path in the two-dimensional surface.

Table 4 Energy levels (in cm^{-1}) and torsional tunneling splittings (in MHz) calculated by the 2D-NS for the 3FBA, 4FBA and BA systems

Level	Energy (3FBA)	Level	Energy (4FBA)	Energy (BA)
0^+	164.0662515	0^+0^+	155.5125144	149.8691346
0^-	164.0662523	0^+0^-	155.5125144	149.8691346
1^+	201.1701021	0^-0^-	155.5268182	149.8842329
1^-	201.1701187	0^-0^+	155.5268182	149.8842329
		Tunneling Splittings		
ΔE_0	0.02		429	453
Exp.	0.82[a]		337.10[b]	492.82[c]
ΔE_1	0.50			

[a] Ref. 13
[b] Ref. 15
[c] Ref. 12

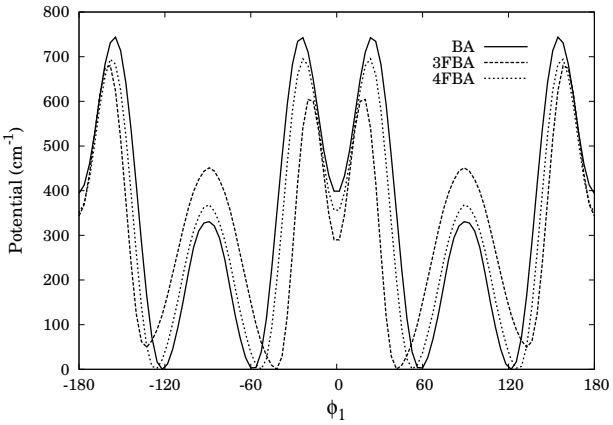

Fig. 3 Potential along the linear reaction path between minima plotted as a function of the torsional angle ϕ_1 (in degrees) for BA (solid line), 3FBA (dashed line) and 4FBA (dotted line). This potential is also represented by lines in the two-dimensional potentials of Figure 2 for the case of 3FBA and 4FBA

The calculated 2D-NS tunneling splitting for 3FBA is 0.02 MHz, whereas the observed tunneling splitting is 0.82 MHz. Although the 2D-NS method correctly predicts that the observed tunneling splitting is very small, the difference between observed and calculated tunneling splittings is quite large. We provide a possible explanation for this discrepancy at the end of the Section.

The 2D-NS ground-state wavefunctions plotted in Figure 4 provide valuable information about the wells involved in the splitting. It should be noticed that the two wavefunctions of the level that splits are symmetric 0^+ (the lowest energy level of the doublet) and antisymmetric 0^- (the highest energy level of the doublet) with respect to the tunneling coordinate, respectively. Both wavefunctions are localized in the two minima 3FBA-M1 and 3FBA-M1*, which clearly demonstrates that the tunneling splitting is due to the interconversion between these two species. Notice that the barrier between M1 and M2 is smaller than the two barriers that separate M1 from M1* by 73 cm^{-1}. However, M2 is 47 cm^{-1} less stable than M1 and this asymmetry avoids the participation of the M2 well in the tunneling splitting. In this context, our calculations are in total agreement with the experimental work of Tang *et al.*[13], who indicated that the observed tunneling splitting is due to the transition between M1 and M1* structures (Z and Z' in their nomenclature). The tunneling splitting is small because the internal rotation involves the passage through the eclipsed configuration with $\phi_1 = 0$ which has a substantial barrier of 525 cm^{-1} for internal rotation. This is consistent with the experimental observation of a c-type transition, which inverts when the -CH_2OH group tunnels from above and below the ring. There is also a substantial rearrangement of the torsions with a change of 86° in ϕ_1 and 116° in ϕ_2.

A somewhat larger tunneling splitting (0.52 MHz) is predicted for the doublet 1^+ and 1^-, which is 47 cm^{-1} above the ground state. The wavefunctions associated to these two energy levels

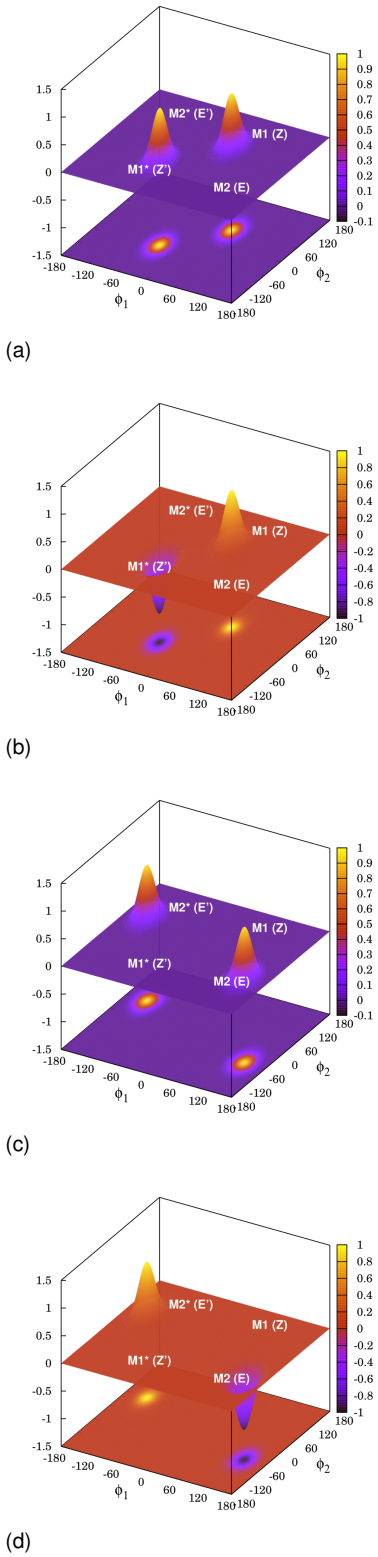

Fig. 4 Three-dimensional representation of the torsional wavefunctions of the 0^+ (a), 0^- (b), 1^+ (c) and 1^- (d) energy levels of 3FBA. The location of the minima is indicated.

lay on M2 and M2*, indicating that first excited state tunneling splitting is due to transitions between these two wells without the participation of M1 or M1*. Localized wavefunctions in isoenergetic wells of the same type, even when there are other wells available, are not exclusive to this case. They were also obtained when studying the tunneling splittings due to the double proton transfer in porphycene.[36]

The cases of BA and 4FBA are different, because the wells M1 and M2 are equivalent, so there are four wells which are isoenergetic. In principle, the four wells may lead to a quadruplet, but the experiments[12,15] showed that only one doublet has been observed. In this case it is possible the conversion between M1 and M1* without passing through the eclipsed configuration which has a higher barrier than the direct interconversion. Bird *et. al*[15] indicated that the observed tunneling splitting of 337.10 MHz must be due to a 60° rotation about ϕ_1 instead of to a 120° rotation. Our calculations show that the former rotation corresponds to the direct interconversion (74° variation in ϕ_1 and barrier of 371 cm^{-1}), whereas the latter is associated to the pass through the eclipsed configuration with a 106° variation in ϕ_1 and a barrier of 603 cm^{-1}. Therefore, the tunneling splitting of 429 MHz calculated by the 2D-NS method in 4FBA follows a direct tunneling path between M1 and M1* in contrast to the case in the 3FBA system. Similarly, in the case of BA the calculated tunneling splitting of 453 MHz, which agrees very well with the experimental value of 492.82 MHz, is a consequence of hindered rotor tunneling between M1 and M1* in the same side of the benzyl ring.

To identify the transitions that lead to the tunneling splitting in BA and 4FBA we have inspected the symmetry of the wavefunctions with respect to the interconversions M1→M1* and M1→M1. Thus, the wavefunctions of the two degenerated ground-state levels depicted in Figures 4(a) and 4(b) are symmetric and antisymmetric, respectively, with respect to the M1→M1 rotation. Both of them are symmetric with respect to the M1→M1* transition, so they are labeled as 0^+0^+ and 0^+0^- in Table 4. This internal rotation does not lead to any tunneling splitting because the barrier height for the M1→M1 transition state is quite high (721 cm^{-1}) and involves a large rotation about ϕ_1. The degenerate levels 0^-0^- and 0^-0^+ with wavefunctions depicted in Figures 4(c) and 4(d) are both antisymmetric with respect to the M1→M1* transition, showing that the tunneling splitting is due to this internal rotation, and in agreement with the experimental findings.

Finally, it is interesting to analyze why the 2D-NS method works well for BA and 4FBA but leads to a splitting which is much too low in the case of 3FBA. The 2D-NS method includes the coupling between the two torsions and incorporates the structural changes in the rests of degrees of freedom through the variation of the reduced moments of inertia (kinetic energy) and of the potential. However, the structural changes may also affect the zero-point energy of the system, whose variation has been neglected in this work. In the case of BA and 4FBA the tunneling splittings are due to motions of the two torsional modes in the same plane of the benzyl ring, with small changes in the rest of the structural parameters, and therefore with minimal changes in the zero-point energy of the remaining degrees of freedom. In the case of 3FBA the tunneling path involves that the rotating groups pass through an eclipsed configuration, which involves an impor-

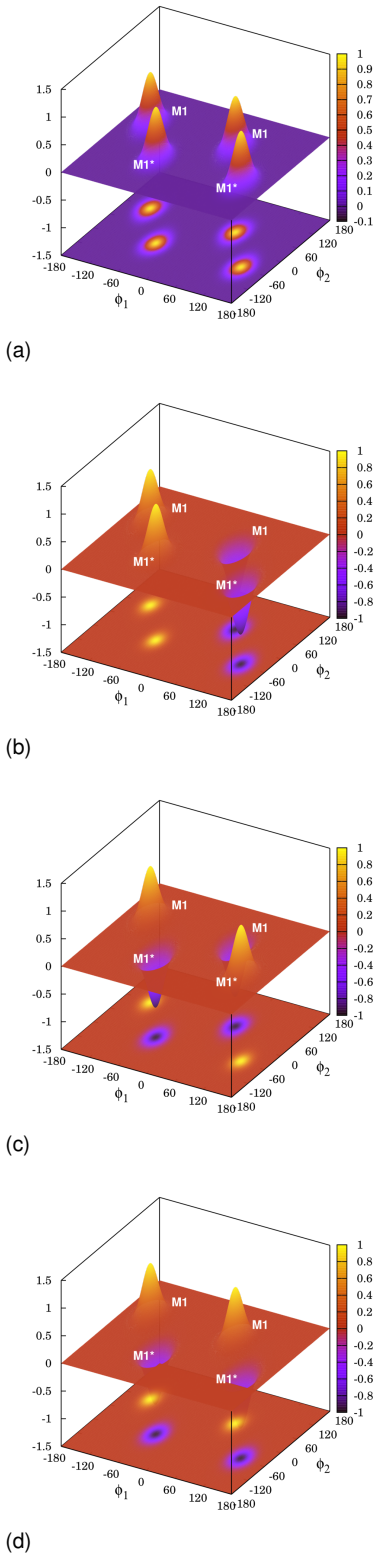

(a)

(b)

(c)

(d)

Fig. 5 Three-dimensional representation of the torsional wavefunctions of the 0^+0^+ (a), 0^+0^- (b), 0^-0^- (c) and 0^-0^+ (d) energy levels of 4FBA. Similar wavefunctions are obtained for BA, and therefore not plotted here. The location of the minima is indicated.

tant rearrangement of some structural parameters. For instance, the OCC angle changes from 109.5° at M1 to 113.1° at M3 and the zero-point energy is 168 cm^{-1} lower in M3 than in M1. This indicates that the barrier between M1 and M3 will probably be lower when the zero-point energy is included and the splitting will increase. The contribution of the zero-point energy of the 3N-8 non-torsional degrees of freedom (where N is the number of atoms) can be included by expressing the force constant matrix in internal coordinates and projecting out the two torsions. This projected zero-point energy can be easily added to the potential of Eq. 2. However, the calculation of the grid of Hessians needed to build this new two-dimensional potential energy surface at the DF-LMP2/cc-pVQZ level is very expensive in computer time, and out of the scope of this work. The search for an efficient incorporation of zero-point energy effects in hindered rotor tunneling splittings is a major task, which we would try to address in future studies.

5 Conclusions

The two-dimensional non-separable (2D-NS) method can be regarded as an extension of one-dimensional methods to study compound rotation in systems with two rotors. It incorporates coupling between the torsions and there is no need to choose a path for tunneling. We have shown that the 2D-NS method is a powerful tool to study hindered rotor tunneling splittings in systems with two coupled torsions if the remaining degrees of freedom do not vary substantially. The methodology was applied to BA and two benzyl alcohol derivatives, i.e., 3FBA and 4FBA. The calculated tunneling splittings of 429 and 453 MHz for 4FBA and BA, respectively, obtained using a torsional potential energy surface calculated at the DF-LMP2-F12//DF-LMP2/cc-pVQZ level and without any empirical adjustment, compare well with the experimental values of 337.10 and 492.82 MHz. The agreement is not as good in the case of 3FBA, with a calculated value of 0.02 MHz versus the experimental value of 0.82 MHz. In this case there are important structural changes of the non-torsional modes, so the variation of the zero-point energy due to these modes may affect the tunneling splitting substantially. This effect is not implemented in current version of the 2D-NS method.

Additionally, the 2D-NS method through the analysis of the wavefunctions provides valuable information about the wells that are involved in the tunneling splitting. We have found that for 3FBA the ground-state splitting is due to tunneling between the M1 and M1* wells passing through an eclipsed configuration, whereas the first excited state tunneling splitting follows the same mechanism but between M2 and M2*. In the case of BA and 4FBA the tunneling path that leads to the tunneling splitting occurs in the same side of the benzyl ring. The ground-state wavefunctions show that the torsional motion M1→M1 does not lead to any splitting and that the observed doublet is due to the interconversion between M1 and M1*.

Acknowledgments

The authors thank W. Siebrand (National Research Council of Canada) and W. Caminati (U. di Bologna) for helpful comments. T. V. A. thanks Fundação de Amparo à Pesquisa do Estado de São Paulo of Brazil for a post-doctoral fellowship. A. F. R. acknowledges funding from Ministerio de Economia y Competitividad of

Spain (Research Grant No CTQ2014-58617-R). F. R. O. thanks the academic support of the Conselho Nacional de Desenvolvimento Científico e Tecnológico (CNPq) of Brazil. A. F. R. and L. S. C. thank the Centro de Supercomputación de Galicia (CESGA) for computacional facilities.

References

1 S. L. Baughcum, R. W. Duerst, W. F. Rowe, Z. Smith and E. B. Wilson, *J. Am. Chem. Soc.*, 1981, **103**, 6296–6303.

2 F. Hund, *Zs. f. Physik*, 1927, **43**, 805–826.

3 Z. Smedarchina, A. Fernández-Ramos and W. Siebrand, *Int. J. Phys. Chem.*, 2001, **22**, 787–801.

4 G. Mil'nikov and H. Nakamura, *Phys. Chem.*, 2008, **10**, 13741393.

5 T. Hammer, M. Coutinho-Neto, A. Viel and U. Manthe, *J. Chem. Phys.*, 2009, **131**, 224109.

6 J. O. Richardson and S. C. Althorpe, *J. Chem. Phys.*, 2011, **134**, 054109.

7 Y. Wang and J. M. Bowman, *J. Chem. Phys.*, 2013, **139**, 154303.

8 Z. Smedarchina, W. Siebrand and A. Fernández-Ramos, *J. Chem. Phys.*, 2012, **137**, 224105.

9 A. Fernández-Ramos, Z. Smedarchina and W. Siebrand, *Phys. Rev. E*, 2014, **90**, 033306.

10 J. O. Richardson, S. C. Althorpe and D. J. Wales, *J. Chem. Phys.*, 2011, **135**, 124109.

11 Z. Smedarchina and F. Zerbetto, *Chem. Phys. Lett.*, 1997, **271**, 189–196.

12 K. A. Utzat, R. K. Bohn, J. A. Montgomery, H. H. Michels and W. Caminati, *J. Phys. Chem. A*, 2010, **114**, 6913.

13 S. Tang, Z. Xia, A. Maris and W. Caminati, *Chem. Phys. Lett.*, 2010, **498**, 52–55.

14 L. Evangelisti, Q. Gou, G. Feng and W. Caminati, *Mol. Phys.*, 2013, **111**, 1994–1998.

15 R. G. Bird, A. E. Nikolaev and D. W. Pratt, *J. Phys. Chem. A*, 2011, **115**, 11369–11377.

16 J. E. Kilpatrick and K. S. Pitzer, *J. Chem. Phys.*, 1949, **17**, 1064.

17 A. Fernández-Ramos, *J. Chem. Phys.*, 2013, **138**, 134112.

18 L. Simón-Carballido and A. Fernández-Ramos, *J. Mol. Model.*, 2014, **20**, 2190.

19 H.-J. Werner, F. R. Manby and P. J. Knowles, *J. Chem. Phys.*, 2003, **118**, 8149–8160.

20 M. Schütz, H.-J. Werner, R. Lindh and F. R. Manby, *J. Chem. Phys.*, 2004, **121**, 737–750.

21 R. Polly, H.-J. Werner, F. R. Manby and P. J. Knowles, *Mol. Phys.*, 2004, **102**, 2311–2321.

22 R. A. Kendall, T. H. Dunning Jr and R. J. Harrison, *J. Chem. Phys.*, 1992, **96**, 6796–6806.

23 F. Weigend, A. Köhn and C. Hättig, *J. Chem. Phys.*, 2002, **116**, 3175–3183.

24 F. Weigend, *Phys. Chem. Chem. Phys.*, 2002, **4**, 4285–4291.

25 F. R. Manby, H.-J. Werner, T. B. Adler and A. J. May, *J. Chem. Phys.*, 2006, **124**, 094103.

26 H.-J. Werner, T. B. Adler and F. R. Manby, *J. Chem. Phys.*, 2007, **126**, 164102.

27 T. B. Adler, H.-J. Werner and F. R. Manby, *J. Chem. Phys.*, 2009, **130**, 054106.

28 *Gnuplot 4.4: an interactive plotting program*, http://gnuplot.sourceforge.net/, 2010.

29 M. Bollhöfer and Y. Notay, *Comput. Phys. Commun.*, 2007, **177**, 951.

30 H.-J. Werner, P. J. Knowles, G. Knizia, F. R. Manby, M. Schütz, P. Celani, T. Korona, R. Lindh, A. Mitrushenkov, G. Rauhut, K. R. Shamasundar, T. B. Adler, R. D. Amos, A. Bernhardsson, A. Berning, D. L. Cooper, M. J. O. Deegan, A. J. Dobbyn, F. Eckert, E. Goll, C. Hampel, A. Hesselmann, G. Hetzer, T. Hrenar, G. Jansen, C. Köppl, Y. Liu, A. W. Lloyd, R. A. Mata, A. J. May, S. J. McNicholas, W. Meyer, M. E. Mura, A. Nicklass, D. P. O'Neill, P. Palmieri, D. Peng, K. Pflüger, R. Pitzer, M. Reiher, T. Shiozaki, H. Stoll, A. J. Stone, R. Tarroni, T. Thorsteinsson and M. Wang, *MOLPRO, Version 2010.1, a package of ab initio programs*, 2010.

31 H. S. Im, E. R. Bernstein, H. V. Secor and J. I. Seeman, *J. Am. Chem. Soc.*, 1991, **113**, 4422–4431.

32 Z. Smedarchina, A. Fernández-Ramos and M. A. Ríos, *J. Chem. Phys.*, 1997, **106**, 3956–3964.

33 W. Siebrand, Z. Smedarchina, M. Z. Zgierski and A. Fernández-Ramos, *Int. Rev. Phys. Chem.*, 1999, **18**, 5–41.

34 J. R. Roscioli, D. W. Pratt, Z. Smedarchina, W. Siebrand and A. Fernández-Ramos, *J. Chem. Phys.*, 2004, **120**, 11351–11354.

35 Z. Smedarchina, W. Siebrand and A. Fernández-Ramos, *J. Phys. Chem. A*, 2013, **117**, 11086–11100.

36 Z. Smedarchina, W. Siebrand and A. Fernández-Ramos, *J. Chem. Phys.*, 2014, **141**, 174312.